Magn Reson Mater Phy
DOI 10.1007/s10334-014-0442-7

RESEARCH ARTICLE

Multi-parametric (ADC/PWI/T2-w) image fusion approach for accurate semi-automatic segmentation of tumorous regions in glioblastoma multiforme

Anahita Fathi Kazerooni · Meysam Mohseni · Sahar Rezaei · Gholamreza Bakhshandehpour · Hamidreza Saligheh Rad

Received: 27 May 2013 / Revised: 11 March 2014 / Accepted: 11 March 2014

Abstract
Object Glioblastoma multiforme (GBM) brain tumor is heterogeneous in nature, so its quantification depends on how to accurately segment different parts of the tumor, i.e. viable tumor, edema and necrosis. This procedure becomes more effective when metabolic and functional information, provided by physiological magnetic resonance (MR) imaging modalities, like diffusion-weighted-imaging (DWI) and perfusion-weighted-imaging (PWI), is incorporated with the anatomical magnetic resonance imaging (MRI). In this preliminary tumor quantification work, the idea is to characterize different regions of GBM tumors in an MRI-based semi-automatic multi-parametric approach to achieve more accurate characterization of pathogenic regions.
Materials and methods For this purpose, three MR sequences, namely T2-weighted imaging (anatomical MR imaging), PWI and DWI of thirteen GBM patients, were acquired. To enhance the delineation of the boundaries of each pathogenic region (peri-tumoral edema, viable tumor and necrosis), the spatial fuzzy C-means algorithm is combined with the region growing method.
Results The results show that exploiting the multi-parametric approach along with the proposed semi-automatic segmentation method can differentiate various tumorous regions with over 80 % sensitivity, specificity and dice score.
Conclusion The proposed MRI-based multi-parametric segmentation approach has the potential to accurately segment tumorous regions, leading to an efficient design of the pre-surgical treatment planning.

Keywords Multi-parametric MRI · Segmentation · Glioblastoma multiforme

Introduction

Glioblastoma multiforme (GBM) brain tumor is the most aggressive form of primary brain tumors with a poor prognosis, for which the survival duration is usually between 6 and 12 months [1]. Magnetic resonance imaging (MRI) has proven to be a powerful tool to provide non-invasive imaging features, such as the extent of tumor invasion and the amount of necrosis and edema, using multiple spectral images. These imaging variables could serve as prognostic indicators of patient survival, which aid in better decision making about the treatment design and improved patient outcome [2]. The extent of necrosis and the amount of peri-tumoral edema have been reported to be negatively correlated with survival [3, 4]. Quantitative assessment of different regions of GBM tumor, namely viable tumor, necrosis, and peri-tumoral edema have shown to be predictive of overall

A. Fathi Kazerooni · S. Rezaei · H. Saligheh Rad (✉)
Department of Medical Physics and Biomedical Engineering, Tehran University of Medical Sciences, Tehran, Iran
e-mail: h-salighehrad@tums.ac.ir

A. Fathi Kazerooni · S. Rezaei · H. Saligheh Rad
Quantitative MR Imaging and Spectroscopy Group, Research Center for Cellular and Molecular Imaging, Tehran University of Medical Sciences, Tehran, Iran

M. Mohseni
Neurosurgery Ward, Imam Khomeini Hospital, Tehran University of Medical Sciences, Tehran, Iran

G. Bakhshandehpour
Paytakht Imaging Center, Tehran, Iran

Published online: 02 April 2014

survival and allow surgeons and neuro-oncologists to determine the necessity of aggressive tumor resection and/or extensive radiotherapy or chemotherapy based on accurate mapping of tumor invasion [5].

Conventionally, the viable tumorous region is defined as the enhancing region observed in the contrast-enhanced T1-weighted (T1-w) images, and the peri-tumoral edema is usually defined as the hyperintensity portion on T2-weighted (T2-w) or FLAIR images, located outside the enhancing area [6]. GBM tumors are highly infiltrative, so, there exists the possibility of tumor invasion in the surrounding tissue and peri-tumoral edema, which, if not resected or destroyed, could increase the probability of tumor recurrence [7]. Also, it is known that GBM tumor is surrounded by a mixture of cytotoxic and vasogenic edema: the former is reversible and could be preserved, while the latter could not be recovered [8]. Although exploiting the mentioned magnetic resonance (MR) imaging modalities could improve the treatment outcome, they can include recoverable tissues (like vasogenic edema) in their tumor detection, while they might miss some parts of tumor infiltration. On the other hand, vasogenic edema in the brain may modestly enhance after contrast administration due to local inflammation in the blood–brain barrier, which makes the local vessels relatively leaky and may be a source of error when one attempts to delineate the exact interface between edema and the tumor in T1-w images with contrast enhancement (T1-w+C).

Numerous recent studies have recommended incorporating additional imaging biomarkers adopted from diffusion-weighted imaging (DWI) and perfusion-weighted imaging (PWI) modalities, which provide deeper insight about the physiological behavior of brain glial tumors [9–11]. The apparent diffusion coefficient (ADC) values calculated by DWI reflect the extent of diffusion restriction in the tissue under investigation: the necrosis and the edematous regions can be identified by higher ADC values. However, T2-w MRI has been reported to be more successful in characterizing the boundaries of peri-tumoral edema than DWI [10, 12]. Despite this, the specified peri-tumoral area on a T2-w image may still contain tumor cells. The regional cerebral blood volume (rCBV) parameter calculated from PWI has shown high correlation with angiogenesis and tumor aggressiveness, and can be used to reliably identify the tumor margins [12].

As the number of images increase, accurate identification of tumorous regions for pre-surgical planning becomes more complicated, time-consuming, prone to intra- and inter-observer variability, and can hardly be reproduced [13]. Recently, several segmentation methods have been proposed for characterization of different brain tumor compartments: region-based active contour models [14–16], clustering-based segmentation techniques, such as k-nearest neighbor [17], knowledge-based fuzzy C-means (FCM) clustering [18–21] or classification approaches [7, 22, 23], which have shown promise in terms of reduced intra- and inter-observer variability and time efficiency [24, 25]. Nevertheless, segmentation of tumor tissues remains a challenging issue, since borders of the heterogeneous tumor and its surrounding tissue are not well-defined in many cases and partial volume effects and MRI inherent noise could complicate the delineation of various regions of the GBM tumor [19]. Considering the aforementioned issues, here we exploit a knowledge-based spatial FCM clustering approach in a multi-parametric (ADC, rCBV-map and T2-w) MRI fusion framework to differentiate various tumorous regions.

Materials and methods

Data acquisition

The images for this experiment were acquired from 13 patients being diagnosed with GBM tumor with histopathological assessment, based on the World Health Organization (WHO) classification system, after MR imaging followed by surgery. The MR data for each patient were acquired on a 3T MR scanner (Siemens MAGNETOM Tim TRIO, Erlangen, Germany) using four-channel 3T Siemens head-coil, with a standard glioma imaging protocol. The protocol consisted of a whole-brain axial T2-w using fast spin-echo sequence with TE/TR = 96/5,000 ms, image matrix = 308 × 384, FOV = 17.6 × 21.9 cm^2, slice thickness = 6 mm; a PWI sequence acquired by a gradient-echo echo-planar imaging sequence with: TE/TR = 45/2,340 ms, flip angle = 60°, image matrix = 128 × 128, FOV = 23 × 23 cm^2, slice thickness = 5 mm, number of measurements = 50 at 1 s/volume and number of slices = 21. The acquisition was performed before and immediately after injection of 15 cc of Gd-DTPA (0.2 mmol/kg) as the contrast agent with a flow rate of 5 ml/s, followed by injection of 20 cc of normal saline solution; and finally a DWI sequence acquired with gradient-echo echo-planar imaging protocol with the following parameters: TE/TR = 137/4,300 ms, image matrix = 192 × 192, FOV = 22 × 22 cm^2, number of slices = 21, slice thickness = 5 mm, *b*-values of 0 and 1,000 s/mm^2 in three orthogonal directions.

Image pre-processing and analysis

Image pre-processing and quantitative map generation

Apparent diffusion coefficient (ADC)-maps were calculated on a voxel-by-voxel basis from the original DW images with software on Siemens imaging workstation. In order to reduce the noise while preserving the edges, an anisotropic diffusion

filter was applied on the T2-w images. Intensity corrections were not performed on PWI images, to not eliminate the bolus signal. PW images were corrected for any possible movement during the imaging session, employing a normalized mutual information affine algorithm, and were then processed by an in-house software package developed in MATLAB2013 (MathWorks, Natick, MA). Brain pixels were isolated from the non-brain pixels in T2-w, DWI and PWI images by generating a brain mask with a skull-stripping algorithm in Statistical Parametric Mapping (SPM8) software (http://www.fil.ion.ucl.ac.uk/spm/) [26]. Quantitative analysis of tissue perfusion was performed employing established tracer kinetic models [27, 28].

Then, T2-w images, ADC and rCBV maps were co-registered using a standard three-dimensional (3D) cubic B-spline transformation algorithm with normalized mutual information cost function in SPM8 software [29].

Semi-automatic segmentation

Knowledge-based spatial fuzzy C-means (FCM) clustering algorithm

Medical images are inherently fuzzy and can be considered as combinations of intensities belonging to the various tissue types beside other unwanted intensities. Thus, it is of paramount importance to take this property into account. Spatial FCM is an unsupervised clustering method utilized in medical image segmentation [30]. This technique tries to iteratively partition the image pixels into C clusters, by minimizing the following cost function:

$$J_{\mathrm{FCM}} = \sum_{m=1}^{C} \sum_{n=1}^{N} \mu_{mn}^{l} \|p_n - c_m\|^2, \tag{1}$$

where N denotes the total number of image pixels, C is the number of clusters, p_n and c_m respectively represent the image pixel and the centroid of the mth cluster, $\|.\|$ is the norm, μ_{mn} is the membership function, which can be computed by:

$$\mu_{mn} = \frac{\|p_n - c_m\|^{-2/(l-1)}}{\sum_{k=1}^{C} \|p_n - c_m\|^{-2/(l-1)}} \tag{2}$$

with $l > 1$ (l controls the degree of fuzziness). The centroids are updated iteratively using

$$c_i = \frac{\sum_{n=1}^{N} \mu_{mn}^{l} i_n}{\sum_{n=1}^{N} \mu_{mn}^{l}} \tag{3}$$

The membership function must satisfy the following relations:

$$\sum_{m=1}^{C} \mu_{mn} = 1, 0 \le \mu_{mn} \le 1, \sum_{n=1}^{N} \mu_{mn} > 0. \tag{4}$$

The algorithm is ideally optimized when high membership values are achieved in pixels with close proximity to the centroid, while pixels that are far apart have low values. In this application, due to heterogeneous GBM tumor margins with surrounding tissue, specifically in the quantitative maps, a knowledge-based FCM algorithm is employed to create several clusters for each image, as follows (Fig. 1):

- T2-w images are classified into four clusters: tissues with hyperintensity values (necrosis), tissues with intermediate intensity (cerebrospinal fluid (CSF) and edema), tissues with hypointensity values (normal white and gray matter, scalp), and with very low or zero intensity (skull, background);
- rCBV maps are classified into two clusters: tissues with high perfusion (including viable tumor), and tissues with low perfusion (including necrosis);
- ADC maps are classified into four clusters: tissues with high ADC values (CSF), with intermediate ADC values (vessels and pathogenic region excluding necrosis), with low ADC (normal white matter, gray matter, and

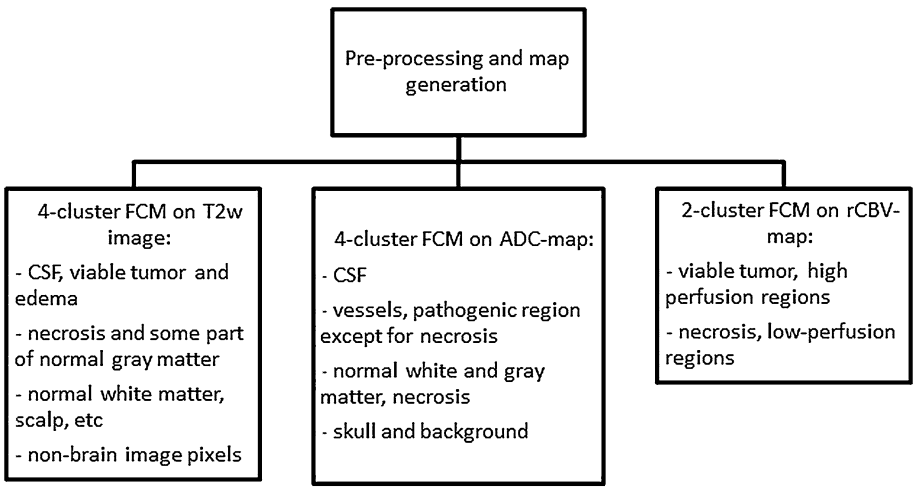

Fig. 1 Schematic flow diagram of knowledge-based tumor clustering. Before clustering, images are pre-processed to eliminate noise, inter-slice motion and to exclude brain tissue from the background. The generated quantitative maps (ADC and rCBV) are registered to the anatomical T2-w images

necrosis), and with very low ADC (background and skull).

Region growing (RG) algorithm

One of the most commonly used region-based methods for image segmentation is the region growing (RG) approach, which starts with selecting *n* seed points. The regions start growing from there by seeking for neighboring pixels meeting the similar criteria as the seed points. The similarity criterion is defined based on texture, homogeneity, topology or other properties of the image. RG method has several advantages in medical image segmentation context, such as its good performance in the presence of noise, the capability to separate the regions with similar properties, and its simple concept [31].

Here, we use RG approach to merge adjacent pixels belonging to the same cluster. We used the criteria of mean intensity of the seed points. The neighboring pixels are added to the current region if their intensities are nearest to the mean of the region and less than a predefined threshold. The initial seed point in the desired cluster is selected manually in the region where the membership degree is one.

FCM–RG method for tumorous tissue characterization

Hereafter, the overall segmentation algorithm is referred to as the FCM–RG method. The procedure is carried out as follows (Fig. 2):

- FCM clustering of the ADC and T2-w images, followed by application of RG with some morphological image processing methods to create individual pathogenic masks (P1 and P2), to be added to generate the final pathogenic mask (P),
- FCM clustering of rCBV map, followed by employing RG to one of the clusters to segment the initial necrosis (N1) and to the other one to separate the initial viable tumorous region (T1),
- Take the intersection of each of N1 and T1 regions with P, to obtain final necrosis (N) and viable tumor (T) masks,
- Exclude the T and N pixels from P, to obtain pure edema area (E), with no tumor invasion.

Ground truth for evaluation

To evaluate the performance of the segmentation algorithm, the MR images were manually segmented by an expert neuroradiologist blinded to the automatic segmentation procedure. The neuroradiologist outlined the borders of each of the tumorous regions for the ground truth assessment based on the widely accepted knowledge: pathogenic region as hyperintense region on the T2-w and ADC map, and tumor vascularization was defined on the rCBV map and the edema as the non-CSF hyperintensity region on T2-w in the periphery of the tumor (compared to the rCBV map). As the manual segmentation was prone to errors (the manually segmented regions could contain overlapping pixels), a

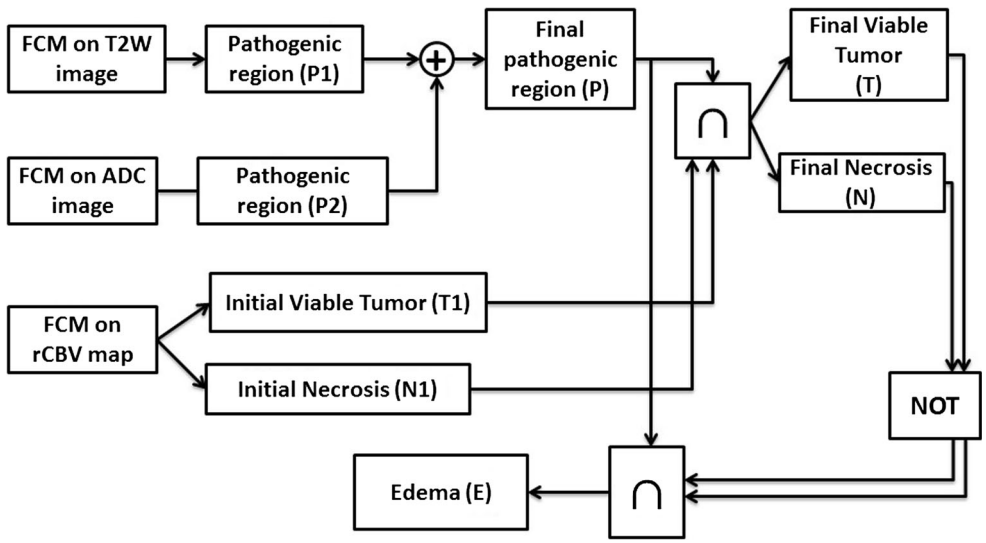

Fig. 2 Schematic flow diagram of the image fusion approach. The overall pathogenic region is obtained by the summation of the segmented pathogenic regions in the T2-w image and ADC map. The initial viable tumor and necrosis regions are segmented out from the rCBV map, and finally segmented by excluding high-perfusion non-tumor regions adjacent to the viable tumor through intersection of the pathogenic region with initial enhancing and necrosis. Then, the pure edema is obtained by separating the necrosis and viable tumor from the overall pathogenic region

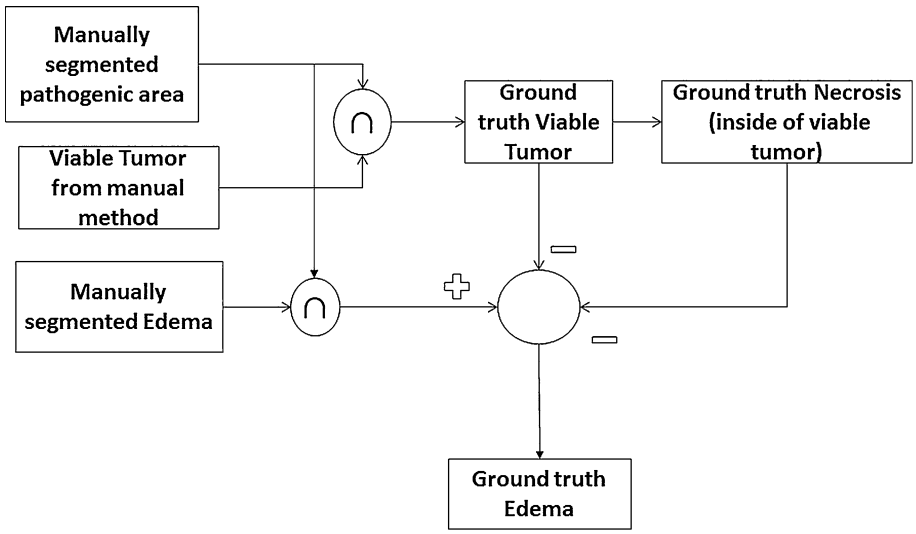

Fig. 3 Schematic flow graph of generating the ground truth segmentation. The manually segmented pathogenic, viable tumor, and necrosis and edema were refined to exclude overlapping pixels based on the illustrated figure

further refinement step was applied (Fig. 3). The refinement was as follows: (1) the overlaps of the segmented tumor vascularization and edema with the pathogenic region were taken, to exclude non-pathogenic tumor or edema regions; (2) the necrosis was specified as the region inside the vascularized tumor; (3) the specified tumor pixels were excluded from the edema region; and finally, (4) the ground truth pathogenic, viable tumor, necrosis, and edema regions were generated. The manual segmentation results were considered as the ground truth. Then, the sensitivity, specificity and Dice similarity criteria [32] were calculated for each case and averaged over all cases to obtain the ultimate values.

Results

Figure 4 illustrates the results of spatial FCM clustering on a T2-w image of one of the cases. Four classes of tissue have been generated: a hyperintensity region including part of necrosis, hypointensity regions including the background and skull, tissues appearing with relatively high signals on T2-w image, such as edema, part of normal gray matter and CSF, and finally tissues with relatively low signal intensity, like white matter and scalp. Similarly, in Fig. 5, the ADC-map is clustered into four classes: high ADC values (like necrosis and parts of CSF), non-brain pixels (background), regions with relatively high ADC values (edema, normal brain tissue, and partly active tumor), and regions with relatively low ADC (normal brain tissue and partly edema and active tumor). Finally, as shown in Fig. 6, the rCBV map is divided into two clusters: one with high rCBV values like viable tumor (angiogenesis) and vessels, and the other one with lower rCBV values like necrosis, edema and normal brain tissue.

Table 1 provides the evaluation results of the spatial FCM–RG method in identifying the whole pathogenic region and several tumorous regions, namely peri-tumoral edema, viable tumor and necrosis. As it can be inferred, the method shows good segmentation outcome (over 80 % of sensitivity, specificity and dice score in almost all of the regions). In Fig. 7, the results of segmentation using FCM–RG in multi-parametric data and the manual segmentation results in one of the cases are illustrated. Figure 7a–c demonstrates the T2-w image and corresponding ADC and rCBV maps, and Fig. 7d–g indicates the segmentation results overlaid on the T2-w image with the delineated borders on Fig. 7(h). The manual segmentation results and the acquired boundaries are illustrated in Fig. 7i–m. It can be observed that the results are visually satisfying.

Discussion

Generally, GBM tumor is heterogeneous and the borders between the tumor and edema are not well defined, and due to tumor infiltration, the edema region could contain tumor cells. Thus, accurate differentiation of the pathological regions becomes difficult. This issue becomes essentially important in pre-surgical treatment planning procedures, where it is important to resect as much of the tumorous tissue as possible, and at the same time, avoid removing uncontaminated tissue [2]. MRI has proven to be a powerful tool to provide diverse information about the patient-specific tumor structure and physiology using multiple spectral images. As a tumor consists of different biological tissues with different appearances on MR images, radiologists usually combine multi-parametric information obtained by multi-spectral MR acquisitions. This process is dependent on

Fig. 4 The results of spatial FCM clustering procedure in T2-w image of a patient (**a**), and four clusters of the tissue: (**b**) hyperintensity regions including necrosis; **c** hypointensity non-brain pixels including skull and background; **d** relatively high signal regions including edema and CSF; and **e** relatively low signal regions comprising normal brain tissue. In these images, the pixel values are continuously scaled from 0 to 1, indicating the degree of pixel membership to each cluster

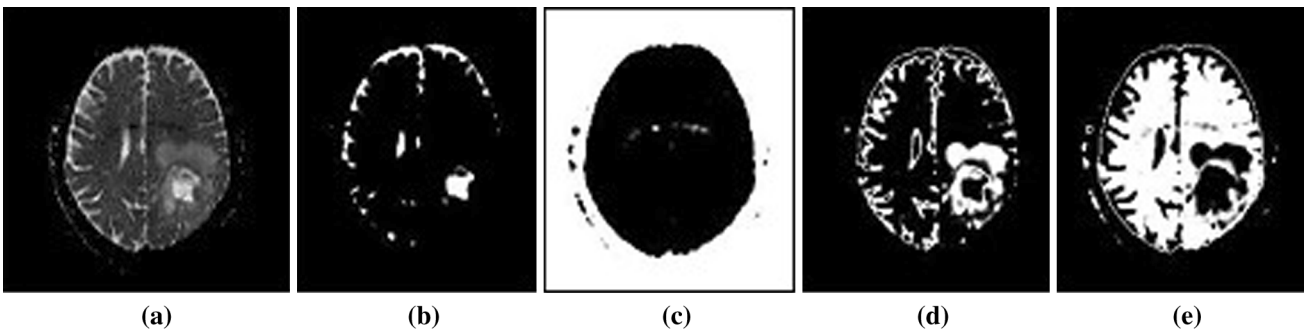

Fig. 5 The results of spatial FCM clustering procedure in ADC-map of a patient (**a**), and four clusters of the tissue: **b** regions with high ADC values including necrosis and partly CSF; **c** non-brain pixels such as background; **d** regions with relatively high ADC values comprising of some parts of CSF and normal gray matter, edema and partly viable tumor; and **e** regions with relatively low ADC values including normal brain tissue, partly viable tumor and edema. In these images, the pixel values are continuously scaled from 0 to 1, indicating the degree of pixel membership to each cluster

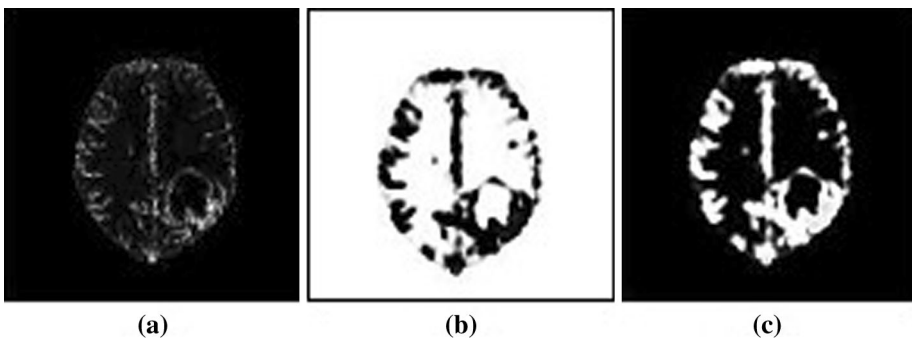

Fig. 6 The results of spatial FCM clustering procedure in rCBV-map of a patient (**a**), and two clusters of the tissue: **b** regions with low rCBV values, including necrosis, normal tissue, and non-brain pixels like background; **c** regions with high rCBV values, like viable tumor and vessels. In these images, the pixel values are continuously scaled from 0 to 1, indicating the degree of pixel membership to each cluster

the manual tracing by a radiology expert in 3D for all MR modalities, which is time-consuming, exhausting and prone to both intra- and inter-rater errors. As the number of images to provide more comprehensive data on a tumor increases, the difficulties with expert-related segmentations become more serious [13]. Hence, accurate and robust tumor segmentation has been a subject of many segmentation studies in recent years, and different segmentation approaches have been carried out and reported in the literature [13, 24].

The proposed glioma segmentation methods can generally be divided into region-based or edge-based,

and clustering or classification approaches, each having potentials and limitations. Region-based or edge-based methods employ a level-set in most of the cases to be evolved toward the tumor boundary by searching for the largest gradient in the image regarding the image intensity or region properties [15]. These methods, while being advantageous in reducing the expert's labor for manual segmentation, rely on the signal intensity and the boundaries of the image objects; hence, they can only be applied on the anatomical images and are not proper to be applied on the parametric maps like ADC maps or rCBV maps. However, numerous studies have reported detection of brain tumor outside the regions specified by conventional MRI [33], which require physiological MRI techniques, such as PWI and DWI to be identified.

Table 1 Evaluation of the segmentation outcomes in each region (using FCM–RG method on multi-parametric data)

	Dice score mean (SD)	Sensitivity mean (SD)	Specificity mean (SD)
Pathogenic	0.89 (0.05)	0.9 (0.02)	0.89 (0.07)
Viable tumor	0.84 (0.06)	0.87 (0.03)	0.83 (0.08)
Necrosis	0.92 (0.04)	0.8 (0.07)	0.98 (0.01)
Edema	0.9 (0.04)	0.87 (0.08)	0.94 (0.03)

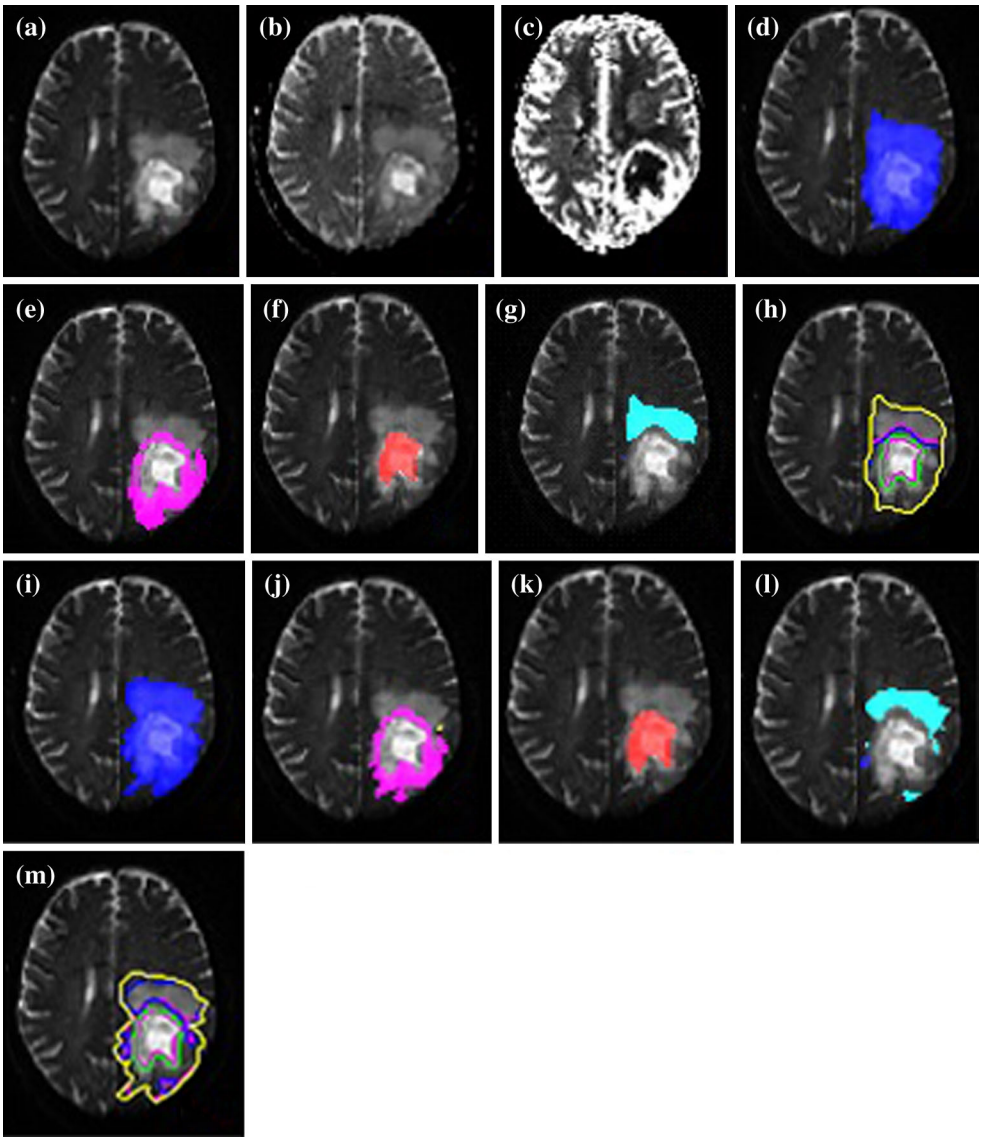

Fig. 7 **a** T2-w image, **b** ADC map (*b*-value = 1,000), **c** rCBV map; segmentation results of the FCM–RG algorithm: **d** pathogenic, **e** viable tumor, **f** necrosis, and **g** edema masks overlaid on T2-w image, **h** the segmentation boundaries (*yellow* pathogenic, *blue* edema, *pink* viable tumor, and *green* necrosis areas); and segmentation results of ground truth segmentation method: **i** pathogenic, **j** viable tumor, **k** necrosis, and **l** edema regions overlaid on T2-w image, **m** the ground truth segmentation boundaries (*yellow* pathogenic, *blue* edema, *pink* viable tumor, and *green* necrosis areas)

Many of the proposed segmentation algorithms are based on classification or clustering approaches, which can handle a pile of information provided by various spectral images. Jensen and Schmainda [7] compared the efficacy of four classifiers to detect brain tumor invasion from structural, diffusion tensor and perfusion images. Verma et al. [34] used a large number of MRI modalities consisting of structural images and diffusion tensor images (DTI) to classify a feature space based on voxel-wise intensity-based feature vectors employing support vector machine (SVM) classifiers. Zollner et al. [35] classified brain tumors by employing support vector machines (SVM) with reduced feature reduction techniques, such as Pearson's correlation coefficients (PCC), principal component analysis (PCA) and independent component analysis (ICA). These approaches have several limitations: (1) they are mostly based on intensity information, and hence require accurate intensity normalization (standardization) and do not incorporate texture and spatial patient-specific information of heterogeneous glioma tumors; (2) they require a large number of modalities, including overlapping information (thus a large feature space) to be incorporated to achieve more reliable segmentation accuracy, and impose a high computational burden, which is not plausible in clinical settings [13]. There have been several attempts to integrate these classification methods with additional constraints, like the work by Weizman et al. [36], which used localization based on an atlas in multi-parametric segmentation in a probabilistic tissue model classification framework. Gooya et al. [37] introduced a joint registration-segmentation approach implemented in GLISTR software for segmentation of brain tumors while the images are registered to an atlas, for which they did not employ functional information from DWI and PWI.

Segmentation of tumor tissues is still a challenge, as the tumors differ greatly in their size, location, tissue heterogeneity and composition (hence different intensity appearance on multiple images). This has been a main motivation for organizers of the Medical Image Computing and Computer Assisted Intervention (MICCAI) conference in the last few years to establish a Multimodal Brain Tumor Segmentation (BRATS) challenge in conjunction with the conference. The BRATS database is composed of structural MR images along with the ground truth segmentation for evaluating and comparing the methods proposed by several researchers in segmenting GBM tumors into various regions, i.e. some of the following regions: complete tumor (tumor core and edema), enhancing tumor, edema and necrosis. As examples, the results of using only the multi-modal structural images have shown Dice overlap of 73 % for complete tumor and 64 % for enhancing tumor by the "Grouping Artificial Immune Network" approach [38], and Dice score of 0.83, 0.7, and 0.75 for complete tumor, tumor core (necrosis, non-enhancing tumor and enhancing tumor) and enhancing tumor, respectively, by using "Random Decision Forests" [38].

By considering the issues of GBM tumor segmentation, here we proposed a knowledge-based multi-parametric fusion technique employing spatial fuzzy clustering to take into account the intensity, spatial and heterogeneous properties of GBM tumors, while incorporating a small number of images providing comprehensive complementary information. Our aim was to use an optimal combination of images with the least possible number of images, while preserving the ability to indicate tumor invasion. The fuzzy models are created based on a priori knowledge provided by expert radiologists: a pathogenic region manifests as a region with hyperintensity on T2-w image, a vascularized viable tumor can be characterized as hyperintensity on an rCBV map (which is superior to post-contrast T1-w image, since the T1-w+C demonstrated blood-brain-barrier leakage as a late ring enhancement, while vasogenic edema may modestly enhance due to the inflammation), and an ADC map could provide additional information about peri-tumoral (both vasogenic and cytotoxic) edema. Finally, a region-growing algorithm is incorporated to fine-tune the coarse segmentation from the spatial fuzzy clustering step. In this step, a region-connection process is applied to merge the adjacent voxels whose membership values belong to the same group.

As the results of quantitative assessment indicate, the proposed method returns more than 80 % of specificity, sensitivity and Dice score in segmentation of different parts of the tumor, which is promising for brain tumor segmentation in comparison with similar works, which employ multi-parametric structural images [38].

Conclusion

In this work, spatial fuzzy C-means (FCM) clustering algorithm was used in combination with region growing (RG) method, referred to as FCM–RG algorithm, to take the fuzzy behavior of the GBM tumor border into account and to take advantage of the RG segmentation method, including its good performance in the presence of noise and capability to correctly separate the regions.

Although the results are promising to detect invading tumor cells, which are not visible on conventional MRI, histological assessment is required to validate the performance of the algorithm in identifying tumor invasion and angiogenesis. Further validation of this work shall be performed by using a larger sample size data, and in order to explore its robustness to inter-patient variations of GBM tumors.

In conclusion, the combination of information provided by anatomical as well as physiological MRI

modalities in a multi-parametric framework (T2-w, PWI and DWI) is beneficial in accurate characterization of pathological regions in GBM brain tumors, which could not be achieved by exclusively using the anatomical MRI.

References

1. Wrensch M, Minn Y, Chew T, Bondy M, Berger MS (2002) Epidemiology of primary brain tumors: current concepts and review of the literature. J Neurooncol 4(4):278–299
2. Pope WB, Sayre J, Perlina A, Villablanca JP, Mischel PS, Cloughesy TF (2005) MR imaging correlates of survival in patients with high-grade gliomas. Am J Neuroradiol 26(10): 2466–2474
3. Hammoud MA, Sawaya R, Shi W, Thall PF, Leeds NE (1996) Prognostic significance of preoperative MRI scans in glioblastoma multiforme. J Neurooncol 27(1):65–73
4. Lacroix M, Abi-Said D, Fourney DR, Gokaslan ZL, Shi W, DeMonte F, Lang FF, McCutcheon IE, Hassenbusch SJ, Holland E (2001) A multivariate analysis of 416 patients with glioblastoma multiforme: prognosis, extent of resection, and survival. J Neurosurg 95(2):190–198
5. Gutman DA, Cooper LA, Hwang SN, Holder CA, Gao J, Aurora TD, Dunn WD, Scarpace L, Mikkelsen T, Jain R (2013) MR imaging predictors of molecular profile and survival: multi-institutional study of the TCGA glioblastoma data set. J Radiol 267(2):560–569
6. Pope WB, Young JR, Ellingson BM (2011) Advances in MRI assessment of gliomas and response to anti-VEGF therapy. Curr Neurol Neurosci Rep 11(3):336–344
7. Jensen TR, Schmainda KM (2009) Computer-aided detection of brain tumor invasion using multiparametric MRI. J Magn Reson Imaging 30(3):481–489
8. Moritani T, Ekholm S, Westesson PL (2009) Diffusion-weighted MR imaging of the brain. Springer, Heidelberg
9. Cha S (2006) Update on brain tumor imaging: from anatomy to physiology. Am J Neuroradiol 27(3):475–487
10. Tofts P (2005) Quantitative MRI of the brain: measuring changes caused by disease. Wiley, London
11. Padhani AR, Miles KA (2010) Multiparametric imaging of tumor response to therapy. J Radiol 256(2):348–364
12. Rollin N, Guyotat J, Streichenberger N, Honnorat J, Minh VAT, Cotton F (2006) Clinical relevance of diffusion and perfusion magnetic resonance imaging in assessing intra-axial brain tumors. J Neuroradiol 48(3):150–159
13. Bauer S, Wiest R, Nolte L-P, Reyes M (2013) A survey of MRI-based medical image analysis for brain tumor studies. J Phys Med Biol 58(13):R97
14. Wang Y, Lin ZX, Cao JG, Li MQ (2011) Automatic MRI brain tumor segmentation system based on localizing active contour models. Adv Mat Res 219:1342–1346
15. Sachdeva J, Kumar V, Gupta I, Khandelwal N, Ahuja CK (2012) A novel content-based active contour model for brain tumor segmentation. J Magn Reson Imaging 30(5):694–715
16. Ho S, Bullitt E, Gerig G (2002) Level-set evolution with region competition: automatic 3-D segmentation of brain tumors. In: Pattern Recognition, 2002. Proceedings. 16th International Conference on 2002. IEEE, pp 532–535
17. Kvinnsland Y, Brekke N, Taxt TM, Grüner R (2009) Multispectral analysis of multimodal images. Acta Oncol 48(2): 277–284
18. Emblem KE, Nedregaard B, Hald JK, Nome T, Due-Tonnessen P, Bjornerud A (2009) Automatic glioma characterization from dynamic susceptibility contrast imaging: brain tumor segmentation using knowledge-based fuzzy clustering. J Magn Reson Imaging 30(1):1–10
19. Dou W, Ruan S, Chen Y, Bloyet D, Constans J-M (2007) A framework of fuzzy information fusion for the segmentation of brain tumor tissues on MR images. Image Vis Comput 25(2):164–171
20. Clark MC, Hall LO, Goldgof DB, Velthuizen R, Murtagh FR, Silbiger MS (1998) Automatic tumor segmentation using knowledge-based techniques. IEEE Trans Med Imaging 17(2):187–201
21. Fletcher-Heath LM, Hall LO, Goldgof DB, Murtagh FR (2001) Automatic segmentation of non-enhancing brain tumors in magnetic resonance images. Artif Intell Med 21(1):43–63
22. Zacharaki EI, Wang S, Chawla S, Soo Yoo D, Wolf R, Melhem ER, Davatzikos C (2009) Classification of brain tumor type and grade using MRI texture and shape in a machine learning scheme. Magn Reson Med 62(6):1609–1618
23. Zikic D, Glocker B, Konukoglu E, Criminisi A, Demiralp C, Shotton J, Thomas O, Das T, Jena R, Price S (2012) Decision forests for tissue-specific segmentation of high-grade gliomas in multi-channel MR. In: Med Image Comput Comput Assist Interv–MICCAI 2012. Springer, pp 369–376
24. Gordillo N, Montseny E, Sobrevilla P (2013) State of the art survey on MRI brain tumor segmentation. J Magn Reson Imaging 31(8):1426–1438
25. Angelini ED, Clatz O, Mandonnet E, Konukoglu E, Capelle L, Duffau H (2007) Glioma dynamics and computational models: a review of segmentation, registration, and in silico growth algorithms and their clinical applications. Curr Med Imaging Rev 3(4):262–276
26. Ashburner J, Friston K (1997) Multimodal image coregistration and partitioning—a unified framework. Neuroimage 6(3): 209–217
27. Østergaard L (2005) Principles of cerebral perfusion imaging by bolus tracking. J Magn Reson Imaging 22(6):710–717
28. Bjørnerud A, Emblem KE (2010) A fully automated method for quantitative cerebral hemodynamic analysis using DSC–MRI. J Cereb Blood Flow Metab 30(5):1066–1078
29. Maes F, Collignon A, Vandermeulen D, Marchal G, Suetens P (1997) Multimodality image registration by maximization of mutual information. IEEE Trans Med Imaging 16(2):187–198
30. Li BN, Chui CK, Chang S, Ong S (2011) Integrating spatial fuzzy clustering with level set methods for automated medical image segmentation. Comput Biol Med 41(1):1–10
31. Hsieh T, Liu Y-M, Liao C-C, Xiao F, Chiang I-J, Wong J-M (2011) Automatic segmentation of meningioma from non-contrasted brain MRI integrating fuzzy clustering and region growing. BMC Med Inform Decis Mak 11(1):54
32. Zou KH, Warfield SK, Bharatha A, Tempany C, Kaus MR, Haker SJ, Wells WM III, Jolesz FA, Kikinis R (2004) Statistical validation of image segmentation quality based on a spatial overlap index: scientific reports. Acad Radiol 11(2):178–189
33. McKnight TR, Noworolski SM, Vigneron DB, Nat ND, Sarah J (2001) An automated technique for the quantitative assessment of 3D-MRSI data from patients with glioma. J Magn Reson Imaging 13(2):167–177
34. Verma R, Zacharaki EI, Ou Y, Cai H, Chawla S, Lee SK, Melhem ER, Wolf R, Davatzikos C (2008) Multi-parametric tissue characterization of brain neoplasms and their recurrence using pattern classification of MR images. Acad Radiol 15(8):966
35. Zöllner FG, Emblem KE, Schad LR (2012) SVM-based glioma grading: optimization by feature reduction analysis. Z Med Phys 22(3):205–214

36. Weizman L, Ben Sira L, Joskowicz L, Constantini S, Precel R, Shofty B, Ben Bashat D (2012) Automatic segmentation, internal classification, and follow-up of optic pathway gliomas in MRI. Med Image Anal 16(1):177–188
37. Gooya A, Pohl K, Bilello M, Cirillo L, Biros G, Melhem E, Davatzikos C (2011) GLISTR: glioma image segmentation and registration. IEEE Trans Med Imaging 31(10):1941–1954
38. http://martinos.org/qtim/miccai2013/